High speed force-volume mapping using atomic force microscope. ‡

Kyong-Soo Kim†   Haiming Wang*   Qingze Zou‡

Mechanical Engineering Department, Iowa State University,   Ames, IA 50011

WANG HAIMING *Abstract*— **This article proposes a control approach based on the notion of superimposition and iterative learning control to achieve high-speed force-volume mapping on scanning probe microscope (SPM). Current force-volume mapping measurement is slow, resulting in large temporal errors in the force mapping when rapid dynamic evolution is involved in the sample. The force-volume mapping speed is limited by the challenge to overcome the hardware adverse effects excited during high-speed mapping, particularly over a relatively large sample area. The contribution of this article is the development of a novel control approach to high-speed force-volume mapping. The proposed approach utilizes the concept of signal decoupling-superimposition and the recently-developed model-less inversion-based iterative control (MIIC) technique. Experiment on force-curve mapping of a Polydimethylsiloxane (PDMS) sample is presented to illustrate the proposed approach. The experimental results show that the mapping speed can be increased by over 20 times.**

I. INTRODUCTION

In this article, an approach based on iterative control to achieve high-speed force-volume mapping on atomic force microscopy (AFM) is proposed. Force-volume mapping, which is to acquire a mapping of local material properties at nanoscale over a sample area, has become an important tool in sciences and engineering fields including biology and materials science [1], [2]. Current force-volume mapping with measurement time generally over 30 minutes, however, is slow [2] and induces large temporal errors into the mapping when the material property to be measured changes rapidly during the mapping. For example, in the elasticity of collagen sample changes rapidly during the dehydration process. The force-volume mapping speed is limited by the challenge to overcome the hardware adverse effects that can be excited during high-speed mapping over a relatively large sample area. The contribution of this article is to propose a high-speed force-volume mapping approach based on signal decoupling-superimposition along with the model-less inversion-based iterative control (MIIC) technique. The proposed method is illustrated by implementing it to obtain the force-curve mapping of a Polydimethylsiloxane (PDMS) sample on one scan line. The experimental results are presented to show that the mapping time can be increased by over 20 times.

Various force-volume mapping techniques have been developed [3], [4]. However, current force-volume mapping methods can not achieve the desired high-speed force-volume mapping. For example, the absolute mode [3], where the force-curve at each sample point was measured from the same initial position with the same (vertical) distance, undesirable excessively large load force can be generated at some points and/or not touching the sample at others. Such issues are avoided in the relative mode, where the same initial load force is applied to the probe before measuring the force-curve at each sample point, as well as when transiting the probe laterally between sample points. However, the sliding of the probe on the sample in this mode is not desirable for soft samples. To avoid such a sliding on the sample, the touch and lift mode [4] has been proposed, where feedback control has been used to determine the load force profile during the force-curve measurement and to lift the probe off the sample afterwards. However, the touch and lift mode is slow in order to compensate for the unknown sample topography variations. In all these above modes, the measurement speed is further limited because during the mapping, the cantilever only moves (relative to the sample) either horizontally (during the transition to the next sample point) or vertically (during the force-curve measurement), but not simultaneously. This horizontal-vertical alternation is avoided by measuring the force curves while continuously scanning the sample in the lateral direction [2]. Although in this method the probe is lifted up after each force curve while the probe is transited to the next sample point, the lateral scanning speed has to be slow (0.1 Hz in [2]) to avoid lateral sliding during the force curve. Clearly, there exist a need to develop new paradigm for achieving high-speed force-volume mapping.

Achieving high-speed force-volume mapping is challenging. The challenge is three-fold: (1) high-speed force-curve measurement at each sample point, (2) rapid transition of the probe from one sample point to the next while compensating for the sample topography difference, with no sliding of the probe on the sample, and (3) seamless integration of the above two motions. These challenges are caused by the adverse effects that can be excited during high-speed force-volume mapping, including the vibrational dynamics of the piezo actuators (used to position the probe relative to the sample) along with the cantilever [5], the nonlinear hysteresis effect of the piezo actuators [6], and the system uncertainties. The vibrational dynamics and the nonlinear hysteresis effects limit the speed of the force-curve measurement (at one sample point) [5], particularly when the vertical displacement of the force-curve is large (in order to lift up the sample and

† E-mail:kyongsoo@iastate.edu.
∗ E-mail: haimingw@iastate.edu.
‡ Corresponding author, E-mail: qzzou@iastate.edu.

in case the required load force is large). Additionally, during the transition of the probe to compensate for the sample topography variation, post transition oscillations can occur [7], particularly at high-speed. Moreover, the motion of the probe (in the vertical direction) needs to switch back and forth between force-curve measurement (at one sample point) and output transition (between current sample point and the next one). Such a switching at high-speed, can also result in large transient oscillatory response due to the mismatch of the state condition at the end of the force-curve measurement and the desired initial state for the point-to-point transition [8]. Therefore, there exist a need to develop new control approach to achieve high-speed force-volume mapping.

The main contribution of the article is the development of a novel switching-motion based force-volume mapping mode. The proposed mode consists of stop-and-go switching motion in lateral scanning, synchronized with the vertical probe motion switching between force-curve measurement and point-to-point output transition. To achieve precision tracking in the lateral scanning as well as in the vertical switching motion, we propose to combine the utilization of the notion of superimposition with the recently-developed MIIC technique [9]. First, the vertical motion of the probe is decoupled as the summation of elements of force-curve measurement at one sample point and elements of output transition at one sample point. Then secondly, the MIIC technique is implemented to obtain the control input to track the element force-curve, and to achieve the element output-transition (at one point) as well. Finally, the control is achieved by superimposing these element inputs together appropriately. A priori sample topography knowledge is utilized in the proposed mode, which can be obtained by using high-speed AFM imaging technique [10]. The proposed method is illustrated by implementing it in experiments to obtain force-volume mapping of a Polydimethylsiloxane (PDMS) sample. The experimental results show that the speed of force-volume mapping can be achieved over 20 times with large lateral scan range (40 μm) and high spatial resolution (128 number of force curves measured per scan line).

II. Iterative Control Approach to High Speed Force Mapping

We start with describing force-volume mapping method and the related control requirements for high-speed mapping. Then we will introduce the proposed force-volume scheme based on switching-motion.

A. Precision control requirements in force-volume mapping

Force volume mapping extends the force-curve measurement at one sample point to obtain a mapping of the force-curves across a sample area [11], [3]. To measure the force curve using AFM, the cantilever is driven by a piezoelectric actuator to approach and touch the sample surface until the cantilever deflection (i.e., the probe-sample interaction force) reaches the set-point value (see Fig. 1). Then the piezoelectric actuator retraces to withdraw the cantilever from the sample surface until the probe surface contact is broken. To obtain a mapping of force-curves over a sample area

(see Fig. 1)—the so called *force-volume mapping*, the force curve is measured at each sample point while the sample is scanned continuously at low-speed under a raster pattern [11]. Feedback control is applied during the force-curve measurement to maintain the same force load and guide the point-to-point probe relocation. The feedback control is to compensate for the sample topography variation from one sample point to the next. Therefore, precision positioning is important in force-volume mapping, because the positioning error during the force-curve measurement at each sample point is directly translated to the errors in the force and/or indentation measurements, and the positioning error in the lateral scanning and in the transition will lead to the coupling of the sample topography into the force.
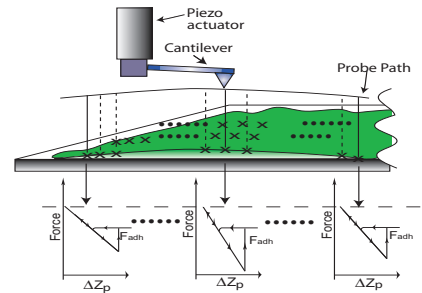

Fig. 1. Concept of force mapping

B. Switching-motion based force-volume mapping

In this article, we propose a switching-motion based force-volume mapping scheme: First, we assume that the sample topography profile has been obtained a priori before the force-volume mapping (for example, through imaging the sample [10]). Then the obtained sample profile will be used to achieve high-speed force-volume mapping. In the proposed force-volume mapping, the lateral *x*-axis scanning trajectory consists of stop-sections and go-sections alternative with each other (see Fig. 2 (a)). Such a stop-and-go switching in lateral scanning will be synchronized with the vertical probe motion as follows: During the stop section (t_m in Fig. 2 (a)), the force-curve will be measured at each sample point, and the probe will be positioned above the sample at the end of the force-curve measurement; then during the subsequent go (transition) section (t_t in Fig. 2 (a)), the AFM-probe will be transited from one sample point to the next, and the sample topography difference between these two sample points will be compensated for. In this method, since the force-curves are acquired with no lateral motion of the probe (relative to the sample), the lateral spatial resolution is improved, particularly at high-speed, over existing force-volume mapping methods [3] with lateral scanning during the force-curve measurement. Moreover, since the sample topography variation is compensated for (through the probe relocation), feedback control is not needed to maintain the same load force profile during the force-curve measurement. Rather, the same input for force-curve measurement can be applied at each sample point. The use of the same input for force-curve at all sample points implies that iterative learning control

techniques can be applied to achieve high-speed in force-curve measurements, as demonstrated in our recent work [5].

1) Switching-motion based trajectory in lateral x-axis scanning: In the proposed approach, the desired stair-like trajectory in the lateral x-axis can be specified as follows: For given lateral scan rate f (in Hz), lateral spatial resolution R (i.e., number of force curves per one scan line), duty ratio $D(\%)$ (i.e., the ratio of the stop-section duration (t_m) relative to the total go and stop duration ($t_m + t_t$), $D = 100 * t_m/(t_m + t_t)$, see Fig. 2 (a)), and the total lateral scan length L, the duration time of the go (transition)-section t_t and that of the stop (measurement)-section t_m, and the lateral spatial distance between two adjacent sample points ℓ_s are determined as below, respectively,

$$t_t = \frac{100 - D}{200 \cdot R \cdot f}, \qquad t_m = \frac{D}{200 \cdot R \cdot f}, \qquad l_s = \frac{L}{\cdot R}. \qquad (1)$$
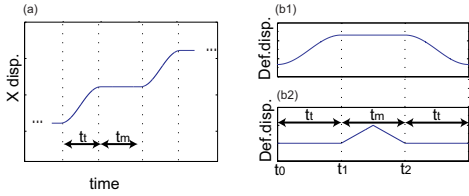
Fig. 2. Basic element of the desired trajectories. (a) X-directional displacement desired trajectory composed of stop (force-curve measurement section) and go (transition section). (b1) Desired deflection the transition trajectory, $z_t(t)$, for point-to-point sample topography variation compensation. (b2) Desired deflection trajectory, $z_m(t)$, for force curve measurement.
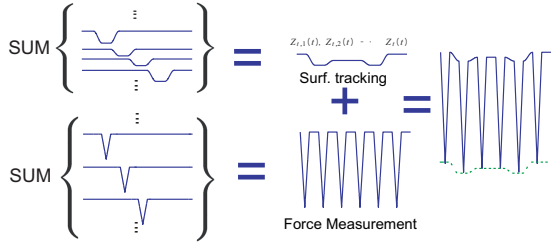
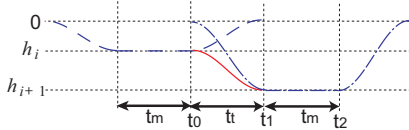Fig. 3. Desired z-axis trajectory generated based on linear superimposition.

Fig. 4. Surface tracking trajectory superimposition. One element of the surface topography tracking signal (dashed line) superimposed on the other element of the surface topography tracking signal (dashed dotted line) generates point to point transition trajectory (solid line).

2) Vertical z-axis trajectory for force-curve measurements and sample topography compensation: In this article, we propose a feedforward control approach that combines offline iterative learning with online implementation via superimposition for the switch-motion based z-axis tracking. First, we decouple the desired z-axis trajectory $z_d(t)$ across the entire scan line, into the trajectory for measuring the probe transition that compensates for the point-to-point sample topography variation, $z_t(t)$, and the trajectory for the force-curves at each sample point, $z_m(t)$, i.e.,

$$z_d(t) = z_t(t) + z_m(t) \qquad (2)$$

Then we will find the feedforward input to track the transition trajectory $z_t(t)$, $u_t(t)$, and the feedforward input to track the force-curves trajectory $z_m(t)$, $u_m(t)$, respectively, through an offline iterative learning method (see Sec. II-C). Provided that the SPM dynamics can be adequately approximated by a linear system around each sample point location, the total input to track the z-axis trajectory $z_d(t)$, $u_z(t)$, can be obtained as

$$u_z(t) = u_t(t) + u_m(t). \qquad (3)$$

The linearization condition holds in the proposed force-volume mapping approach provided that enough points are sampled along the scan line—as needed to achieve high resolution in the force-volume mapping. Moreover, the hysteresis effect will be effectively addressed through offline iterations in the proposed approach. Based on the above trajectory decoupling (Eq. (2)), we further decouple the desired transition trajectory $z_t(t)$ as a summation of one-point transition $z_{t,i}(t)$ with different transition range (see Fig. 3 and 4) :

$$z_t(t) = \sum_{i=1}^{R} h_i z_{t,i}(t - i * T_s), \qquad (T_s \triangleq t_t + t_m) \qquad (4)$$

where R is the lateral spatial resolution defined before, h_i denotes the scale factor for the one-point transition, and $z_{t,i}(t)$ denotes the transition trajectory element selected from a library for the transition at the ith sample point, i.e., the library consists of trajectory elements for one-point transition with different transition ranges, which will be constructed offline a priori. Thus, in implementations, the entire sample topography trajectory across each scan line will be obtained a priori and then partitioned by the total number of sample points to determine the selection of the one-point transition element $z_{t,i}(\cdot)$. Additionally, the one-point transition element $z_{t,i}(\cdot)$ comprises an up-transition section and a down-transition, connected by a stop (flat) section in between (see Fig. 4)—during the flat section, force curve will be measured. The inclusion of both up- and down- transition sections renders the same initial and post state condition, which facilitates the use of iterative control to track such a trajectory. The up- and down- transition sections are designed by using cosine functions.

$$\begin{aligned} & \frac{h_i}{2}[cos(\omega(t - t_0)) + 1] + \frac{h_{i+1}}{2}[cos(\omega(t - t_0) + \pi) + 1] \\ = & \frac{h_i - h_{i+1}}{2}cos(\omega(t - t_0)) + \frac{h_i + h_{i+1}}{2} \end{aligned} \qquad (5)$$

where h_i and h_{i+1} denotes the partitioned transition height at the ith and the $i+1^{th}$ sample point, respectively.

Similarly, the force-curve measurement trajectory $z_m(t)$ is also decoupled as a summation of individual force-curves at each sample point as follows (see Fig. 2):

$$z_m(t) = \sum_{i=1}^{R} z_{m,i}(t - i * T_s), \qquad (T_s \triangleq t_t + t_m) \qquad (6)$$

where $z_{m,i}(t)$ denotes force curve measurement at the ith sample point. Note that in the proposed approach, the control input to track the one-point transition trajectory

element $z_{t,i}(t)$, $u_{t,i}(t)$, and the input to track the individual force-curve $z_{m,i}(t)$, $u_{m,i}(t)$ will be obtained a priori through offline iterations (see Sec. II-C). Therefore, the input for the point-to-point transition, $u_t(t)$, is obtained by superimposing the inputs for one-point transitions together—according to Eq. (4) and the input for the force-curve measurements, $u_m(t)$ is obtained similarly via superimposition by Eq. (3).

Lemma 1: Let $u_{t,i}(\cdot)$ be the feedforward control input to track the one-point transition element $z_{t,i}(\cdot)$, and $u_{m,i}(\cdot)$ be the feedforward control input to track the one-point force curve element $z_{m,i}(\cdot)$, then the linearly superimposed input $u_z(t)$ as specified by Eqs. (3,4,6) will track the superimposed trajectory $z_d(t)$.

Proof The Lemma follows by the superimposition property of linear dynamics system. ∎

Remark 1: As shown through the development of the stable-inversion theory [12], the feedforward inputs to track the one-point transition element, $u_{t,i}(\cdot)$, and that to track the one-point force-curve element, exist, even for nonminimum-phase systems like many piezoactuators. Such a feedforward input for nonminimum-phase systems requires the input to be applied before the output change occurs—pre-actuation (or equivalent, preview- actuation). The needed preview time can be determined by using the force-curve element at the first sample point.

Remark 2: As the element trajectories, $z_{t,i}(\cdot)$ and $z_{m,i}(\cdot)$, are known a priori, it has been established that iterative control approach is highly effective in achieving precision tracking of such pre-known trajectories in practices.

C. Model-less Inversion-based Iterative Control (MIIC)

The MIIC algorithm [9] is given below,

$$u_0(j\omega) = \alpha y_d(j\omega), \qquad k = 0,$$

$$u_k(j\omega) = \begin{cases} \frac{u_{k-1}(j\omega)}{y_{k-1}(j\omega)} y_d(j\omega), & \text{when } y_k(j\omega) \neq 0 \\ & \text{and } y_d(j\omega) \neq 0 \quad k \geq 1, \quad (7) \\ 0 & \text{otherwise} \end{cases}$$

where $\alpha \neq 0$ is a pre-chosen constant (e.g., α can be chosen as the estimated DC-Gain of the system).

The next theorem discusses the convergence of the MIIC algorithm upon the additional disturbance and/or measurement noise.

Theorem 1: Let the system output $y(j\omega)$ is effected by the disturbance and/or the measurement noise as

$$y(j\omega) = y_l(j\omega) + y_n(j\omega), \qquad (8)$$

where $y_l(j\omega)$ denotes the linear part of the system response to the input $u(j\omega)$, i.e. $y_l(j\omega) = G(j\omega)u(j\omega)$, and $y_n(j\omega)$ denotes the output component caused by the disturbances and/or measurement noise, at frequency ω,

1) assume that during each iteration, the NSR is bounded above by a positive, less-than-half constant $\varepsilon(\omega)$, i.e.,

$$\left| \frac{y_{k,n}(j\omega)}{y_d(j\omega)} \right| \leq \varepsilon(\omega) < 1/2, \quad \forall \ k \qquad (9)$$

then the ratio of the iterative input to the desired input is bounded in magnitude and phase, respectively, as

$$R_{\min}(\omega) \leq \lim_{k \to \infty} \left| \frac{u_k(j\omega)}{u_d(j\omega)} \right| \leq R_{\max}(\omega), \qquad (10)$$

where $R_{\min}(\omega) \triangleq 1 - \varepsilon(\omega)$ and $\frac{1-\varepsilon(\omega)}{1-2\varepsilon(\omega)} \triangleq R_{\max}(\omega)$,

$$\lim_{k \to \infty} \left| \angle \left(\frac{u_k(j\omega)}{u_d(j\omega)} \right) \right| \leq \sin^{-1} \left(\frac{\varepsilon(\omega)}{1-\varepsilon(\omega)} \right) \triangleq \theta_{\max}(\omega) \qquad (11)$$

and the relative tracking error is bounded as

$$\lim_{k \to \infty} \left| \frac{y_k(j\omega) - y_d(j\omega)}{y_d(j\omega)} \right| \leq \frac{2\varepsilon(\omega)(1-\varepsilon(\omega))}{1-2\varepsilon(\omega)}; \qquad (12)$$

III. EXPERIMENTAL EXAMPLE: ELASTICITY AND ADHESION FORCE VOLUME MAPPING ON A LINE

In this section, we illustrate the MIIC technique by implementing it in the output tracking of a piezotube actuator on an AFM system. system first.

A. Experimental setup

The schematic diagram of the experimental AFM system (Dimension 3100, Veeco Inc.) is shown in Fig. 5 for the control of the x-axis piezotube actuator. All the control inputs to the piezo actuator were generated by using MATLAB-xPC-target package, and sent out through a data acquisition card (DAQ) to drive the piezo actuator via an amplifier.The AFM-controller had been customized so that the PID control circuit was bypassed when the external control input was applied.
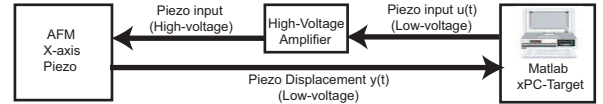

Fig. 5. Schematic diagram of the experiment setup to implement the proposed MIIC algorithm

B. Implementation of the Switching-motion-based force-volume mapping

The proposed switching-motion based force-volume mapping is illustrated by using a PDMS sample as an example. The stair-like desired trajectory for the lateral x-axis scanning was specified first. The scan size was chosen at $40\mu m$, and a total of 128 force curves were measured per scan line (i.e., R = 128). Moreover, two different duty ratios (D = 20 and 50) for the stop-and-go section of each stair in the x-axis trajectory (see Sec. II-B.1), along with three different x-axis lateral scan rates (f = 0.5, 1, 2 (Hz)), were chosen in the experiments. Therefor, the transition time t_t, the measurement time t_m, and the point-to-point spatial distance ℓ_s, are also specified accordingly (see Sec. II-B.1). For example, for the the case of 2 Hz lateral line scan speed and duty ratio of D=20, the transition time ($t_t = 1.563$ ms), the measurement times ($t_m = 0.39$ ms), and the point-to-point spatial distance ($l_s = 313nm$) were determined. Once the x-axis desired trajectory was determined, the z-axis desired trajectory can be determined accordingly. Particularly, the total trajectory for the force-curve measurements ($z_m(t)$ in Eq. (6)) was designed by choosing the vertical displacement of each force-curve element ($z_{m,i}$ in Eq. (6)) as 800 nm. As shown in Fig. 2 (b2), each force-curve consisted of a triangle trajectory followed by a flat section, and to be synchronized with x-axis motion, the duration of the triangle part and the duration

of the flat part were equivalent to the measurement time t_m and the transition time t_t, respectively. The triangle part was symmetric with the same push-in time and the pull-up time. Similarly, the total trajectory for the point-to-point transition ($z_{t,i}$ in Eq. (4)) was designed by specifying the one-point transition element also. In this experiment, we simplified the design of the library of elements for one-point transitions (see Sec. II-B.2 and Eq. (4)) by having only one element for one-point transition. Specifically, the element for one-point transition was chosen to have a displacement range of 98 nm, corresponding to one voltage displacement sensor output. Then the total transition trajectory was determined by scaling the one-point transition element according to the transition height at each sample point (see Eq. 4 and Sec. II-B.2). Next, the MIIC control algorithm was used to find, ahead of time, the converged inputs for tracking the stair-like x-axis desired trajectory, and then the force-curve element along with the one-point transition element, respectively. The obtained control inputs were stored and applied appropriately during the force volume mapping on one scan line (such that the switching-motion in the lateral scanning was synchronized with the force-curve and transition switching in the vertical direction). We demonstrated the technique by measuring the force-volume mapping on one scan line, and the sample topography profile was obtained a priori by iteratively using the absolute mode force-curve measurement along the scan line.

C. Experimental Results & Discussion

1) Experimental output tracking results: The output tracking results achieved by using the MIIC control technique are compared with those obtained by using the DC-Gain method in Figs. 6 for the tracking of the stair-like x-axis trajectory and the tracking of the force-curve element and the one-point transition element. In the DC-Gain method, the control input was obtained by scaling the desired output with the DC-Gain of the system. Therefore, the DC-Gain method did not account for the dynamics of the system, and the obtained output tracking quantitatively demonstrate the effects of the SPM dynamics on the positioning precision. In Fig. 6, the tracking results are shown for the scan rates of 2 Hz with duty ratio D = 20, where the load rate of the force-curve equaled to 4.1 mm/s. (Experimental results for the other 5 different scanning and duty combinations were omitted due to the page limits). When implementing the MIIC technique, the iteration was stopped when neither the relative RMS-tracking error nor the relative maximum-tracking-error decreased further. The resulting tracking results are shown in Table. I in terms of the relative RMS error $E_2(\%)$ and the relative maximum error $E_\infty(\%)$, as defined below,

$$E_2(\%) \triangleq \frac{\|y_d(\cdot) - y(\cdot)\|_2}{\|y_d(\cdot)\|_2} \times 100\%, E_\infty(\%) \triangleq \frac{\|y_d(\cdot) - y(\cdot)\|_\infty}{\|y_d(\cdot)\|_\infty} \times 100\%. \quad (13)$$

The experimental results show that precision tracking in the proposed switching-motion based force-volume mapping can be achieved by using the MIIC technique. As shown in Fig. 6 and Table I, when the lateral scan rate and the load-rate of the force-curves were relatively low, the dynamics

TABLE I

TABLE I

TRACKING ERRORS BY USING THE MIIC TECHNIQUE FOR THE x-AXIS TRAJECTORY, THE FORCE-CURVE ELEMENT, AND THE ONE-POINT TRANSITION ELEMENT. THE RMS ERROR $E_2(\%)$ AND THE MAXIMUM ERROR $E_{max}(\%)$ ARE DEFINED IN EQ. (13). APPROACHING RATE IS IN UNIT OF mm/s.

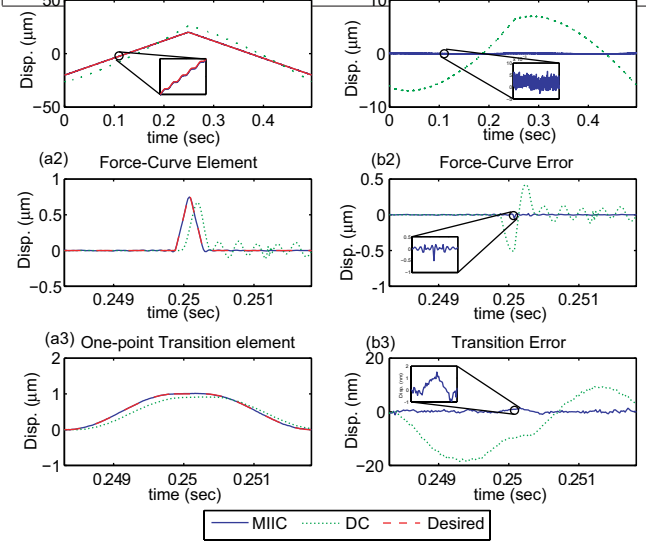| Scan Rate	Duty Rate	App. Rate	E_2 (%)			E_{max} (%)		
			X	Z_m	Z_t	X	Z_m	Z_t
0.5 Hz	20	1.02	0.77	3.76	1.17	0.63	1.51	2.94
0.5 Hz	50	0.41	1.16	0.65	3.38	0.45	2.34	1.18
1 Hz	20	2.05	1.16	1.69	0.98	0.5	3.95	3.06
1 Hz	50	0.82	1.74	0.7	0.92	0.44	2.51	2.93
2 Hz	20	4.1	1.92	3.55	0.67	0.39	6.33	1.72
2 Hz	50	1.64	2.95	1.03	0.68	0.35	9.95	1.79

Fig. 6. Experimental tracking results for the scan rate of 2 Hz, and the duty ratio D = 20, where the load rate of the force-curve equaled to 4.1 mm/s.
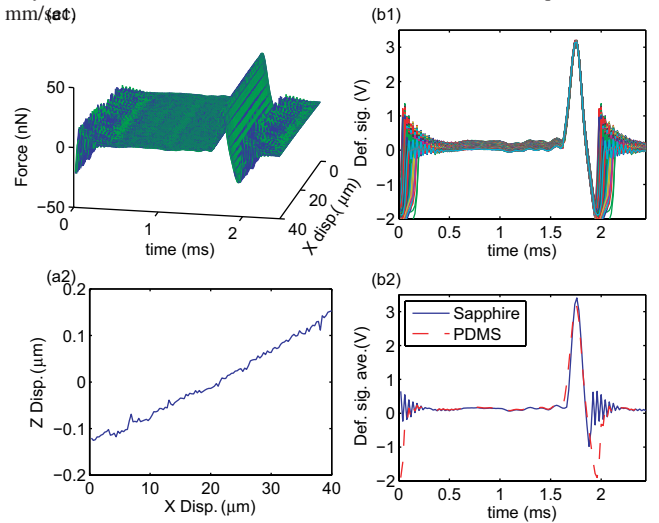

Fig. 7. (a1) The 3-D plot and (b1) the side view of the force-volume mapping on the PDMS sample, (a2) the sample topography across the scan line, and (b2) the comparison of the force-time curve on the PDMS with that on a sapphire sample. The load rate is $4.1 mm/s$.

effect was small, thereby the tracking errors of the force-curve element and the one-point transition element by using the DC-gain method were relatively small (around 5%). Instead, due to the large lateral scanning range (40 μm), the hysteresis effect was pronounced (see Fig. 6 (a1), (b1)).

However, by using the proposed MIIC technique, such a large hysteresis effect was substantially removed (as shown in Fig. 6 (b1) and Table I, the tracking error was cless than 3%), and so were the error in the force-curve element and the one-point transition element tracking (see Fig. 6 (a2) to (b3)). Therefore, the experimental results show that precision tracking in the proposed switching-motion based force-volume mapping can be achieved by using the MIIC technique.

2) Force-Volume Mapping of a PDMS Sample: The converged control inputs to the tracking of the x-axis and the z-axis trajectories, obtained above, were apply to measure the force-volume mapping on a PDMS sample. The PDMS sample was prepared as describe in [13]. The preparation process ensured that the PDMS sample is homogeneous, i.e., the mechanical properties of the sample remained almost the same across the entire sample area. First, the sample topography was obtained as described earlier, then the obtained sample topography was partitioned by using the lateral spatial resolution (R = 128), which was then used to determine the scale factor h_i for the control input to the one-point transition element at each sample point. Then the z-axis control input was obtained via superimposition as described in Sec. II-B.2, and was synchronized with the x-axis control input during the implementation. The obtained force-volume mapping results over one scan line are shown in Fig. 7 for the line scan rate of 2 and the force rate of 4.1 mm/sec.

The experimental results show that force-volume mapping speed can be significantly improved by using the proposed approach. As shown in Fig. 7 (a1), the force-curves measured at all sampled points were very close to each other, which is even more clear in the side-view of the force-volume mapping result in Fig. 7 (b1). Such a uniformity across the sampled point implied that the mechanical properties at all sampled points were very close to each other, i.e., the PDMS sample was homogeneous. Thus, the measured force-volume mapping results agree with our expectation. We note that such measurement results were achieved when there existed significant sample topography variation across the 40 μm scan line—-as shown in Fig. 7 (a2). Thus, the experimental results showed that the proposed method can effectively remove the sample topography effect on the force-volume mapping when the scan rate and the force load rate were relatively low. Such an ability, to remove the sample topography effect on the force-volume mapping, was maintained even when the scan rate and the force load rate were increased by 10-fold, as shown in Fig. 7. Finally, we also compared the force-curves measured on the PDMS sample with those measured on the Sapphire sample for the same control input at the load rate of 4.1 mm/sec, as shown in Fig. 7 (b2), respectively. The obtained experimental results show the rate-dependent elastic modulus of PDMS [13]. Note the slope of the force-curves shown in Fig. 7 (b2) is proportional to the elastic modulus of the material [14]. When the load-rate was slow, the PDMS sample tended to behave softer with a lower elastic modulus, i.e., the slope of the force curve is smaller. As the load rate was increased,

the PDMS sample tended to behave stiffer with a higher elastic modulus, i.e., the slope of the force curve was larger and close to that of sapphire—as shown in Fig. 7 (b2). Such a trend agrees with our recent results reported in [13]. Therefore, the experimental results illustrate the efficacy of the proposed approach to achieve high-speed force-volume mapping.

IV. CONCLUSIONS

In this article, high-speed force-volume mapping using switching-motion based force-volume mapping mode and model-less inversion based iterative control technique on atomic force microscopy is presented. The proposed approach was based on signal decoupling-superimposition and the elemental input signals were found by MIIC technique. The proposed methods is implemented to obtain the force-curve mapping of a PDMS sample on one scan line. The experimental results were presented and showed that the force mapping speed with precision force curve measurement can be increased by over 20 times.

REFERENCES

[1] C. Rotsch and M. Radmacher, "Drug-induced changes of cytoskeletal structure and mechanics in fibroblasts: An atomic force microscopy study," *Biophysical Journal*, vol. 78, pp. 520–535, 2000.

[2] H. Suzuki and S. Mashiko, "Adhesive force mapping of friction-transferred ptfe film surface," *Applied Physics A:Materials Science & Processing*, vol. 66, pp. S1271–S1274, 1998.

[3] M. Radmacher, J. P. Cleveland, M. Fritz, H. G. Hansma, and P. K. Hansma, "Mapping interaction forces with the atomic force microscope," *Biophysical Journal*, vol. 6, pp. 2159–2165, 1994.

[4] B. Cappella, P. Baschieri, C. Frediani, P. Miccoli, and C. Ascoli, "Improvements in AFM imaging of the spatial variation of force-distance curves: on-line images," *Nanotechnology*, vol. 8, pp. 82–87, 1997.

[5] K.-S. Kim, Q. Zou, and C. Su, "A new approach to scan-trajectory design and track: AFM force measurement example," *ASME Journal of Dynamic Systems, Measurement and Control*, vol. 130, p. 151005, 2008.

[6] Q. Zou and Y. Wu, "Iterative control approach to compensate for both the hysteresis and the dynamics effect of piezo actuators," *IEEE Trans. on Control Systems Technology*, vol. 15, 2007.

[7] M. A. Lau and L. Y. Pao, "Input shaping and time-optimal control of flexible structures," *Automatica*, vol. 39, pp. 893–900, 2003.

[8] A. Serrani, A. Isidori, and L. Marconi, "Semiglobal nonlinear output regulation with adaptive internal model," *IEEE Trans. on Automatic Control*, vol. 46, pp. 1178–1194, 2001.

[9] K.-S. Kim and Q. Zou, "Model-less inversion-based iterative control for output tracking: Piezo actuator example," 2008.

[10] Y. Wu, Q. Zou, and C. Su, "A current cycle feedback iterative learning control approach to afm imaging," (Seattle, WA), pp. 2040–2045, June 2008.

[11] H.-J. Butta, M. Jaschkea, and W. Duckerb, "Measuring surface forces in aqueous electrolyte solution with the atomic force microscope," *Bioelectroehemistry and Bioenergetics*, vol. 38, pp. 191–201, 1995.

[12] Q. Zou and S. Devasia, "Precision preview-based stable-inversion for nonlinear nonminimum-phase systems: The VTOL example," *Automatica*, vol. 43, pp. 117–127, 2007.

[13] K.-S. Kim, Z. Lin, P. Shrotriya, and S. Sundararajan, "Iterative control approach to high-speed force-distance curve measurement using AFM: Time dependent response of pdms," *UltraMicroScopy*, vol. 108, 2008.

[14] H.-J. Butt, B. Cappella, and M. Kappl, "Force measurements with the atomic force microscope: Technique, interpretation and applications," *Surface Science Reports*, vol. 59, pp. 1–152, 2005.